Direct correspondence between HEB current-voltage characteristics and the current-dependent resistive transition

R. Barends[1], M. Hajenius[1,2], J.R. Gao[1,2], and T.M. Klapwijk[1]

[1]Kavli Institute of NanoScience, Faculty of Applied Physics, Delft University of Technology, Lorentzweg 1, 2628 CJ Delft, The Netherlands.
[2]SRON National Institute for Space Research, Sorbonnelaan 2, 3584 CA Utrecht, The Netherlands.

***Abstract*— Currently, superconducting hot electron bolometer mixers are the most promising candidates for heterodyne detection above 1 THz. The core of its bolometric operation is the resistive transition of the superconductor. In the past device transitions, parameterised by sigmoidal transitions, entered modelling equations, and proved insufficient to adequately predict current voltage characteristics. Recently we have experimentally observed the intrinsic film transition to be different from the device transition. We analyse the role of the current dependent intrinsic transition and qualify device response, focussing on operating conditions, using a distributed numerical model based on the electron and phonon temperature and the local resistivity. Including the current dependence results in an excellent agreement between predicted and measured pumped $I(V)$, and a modification of the local resistivity, leading to a new view on the device response.**

I. Introduction

Hot electron bolometer mixers have evolved to a valuable addition to the astronomical community, being ideally suited for low noise heterodyne detection above 1 THz. Under operation, due to radiation and bias, the electrons are heated and induce local resistance. The exact shape of temperature and resistivity profiles results from a delicate interplay between thermal mechanisms, contact issues and local resistivity.

In this interplay the response of the superconductor to the electron temperature, the resistive transition, plays a pivotal role. Earlier, sigmoidal transitions, approximating the device transition, have been shown to be valuable for qualifying the device response to radiation and bias [5], and to provide insight in its mixing mechanism [1].

Still, the intrinsic resistive mechanisms remained underexposed, being veiled by contact effects. Recently, we have shown that the intrinsic film transition, measured on a film without usual contact structure, has a much sharper onset [2].

For analysing the influence of the resistive transition in order to describe more correctly recent device results we have performed a comprehensive numerical analysis, using a distributed heat balance. Qualitatively it is found that a current-dependent local oscillator power induced bell-shaped curve rises with increasing bias, which forms the framework from which the device current-voltage characteristics can be derived.

II. Heat Balance

Under operating conditions, primarily LO power and secondarily DC power induce a temperature profile, which in turn leads to a resistivity profile. As such, we are interested in time-independent processes. The specific shape of these profiles is determined using a one-dimensional distributed heat balance, which takes the form of a coupled differential equation for the electron temperature T_e and phonon temperature T_p,

$$\begin{aligned} \frac{d}{dx}(\lambda_e \frac{d}{dx} T_e) + p - p_{ep} &= 0, \\ \frac{d}{dx}(\lambda_p \frac{d}{dx} T_p) + p_{ep} - p_{ps} &= 0, \end{aligned} \tag{1}$$

in which $\lambda = cD$ denotes a thermal conductance, with D the diffusivity; and p the DC and RF power absorbed per unit volume, $p = p_{DC} + p_{RF}$, with the DC power absorption depending on the local resistivity ρ, $p_{DC} = J^2\rho$. The power transfers between electron and phonon subsystems, and subsequently the substrate are denoted by p_{ep} and p_{ps},

$$\begin{aligned} p_{ep} &= \frac{c_e}{n\tau_{ep} T_e^{n-1}} (T_e^n - T_p^n) \\ p_{ps} &= \frac{c_p}{m\tau_{esc} T_p^{m-1}} (T_p^m - T_b^m) \end{aligned} \tag{2}$$

with the powers $n = 4$ and $m = 4$ for our case [8]. The electron temperature dominates over the phonon temperature in determining device response.

The one-dimensional approach is motivated by the skin depth and the magnetic penetration depth being larger than or of the same magnitude as the device width. Since also $hf \gg 2\Delta$ the LO power absorption is assumed uniform. The assumption of full thermalisation, and thus describing the thermal properties in terms of an electron temperature is allowed, since the inelastic electron-electron interaction length, typically around 10 nm, is smaller than the device length. The electron-phonon interaction time being smaller than the phonon escape time, $\tau_{ep} < \tau_{esc}$, and the wavelength of a thermal phonon $\lambda_T = \frac{hu}{k_B T_p}$, typically around 20 nm, being smaller than the device length motivates the usage of the phonon temperature.

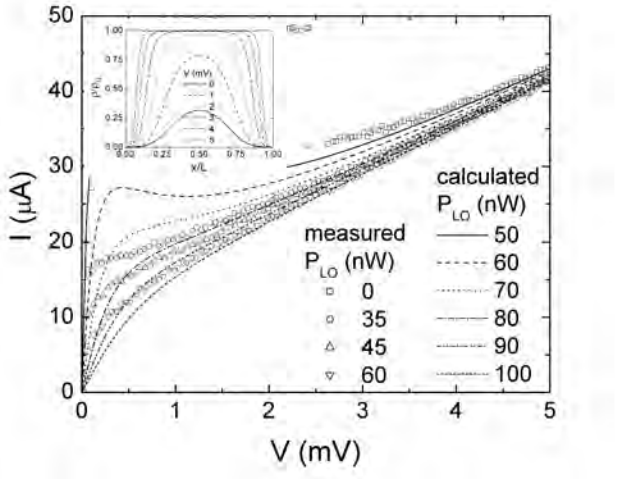

Fig. 1. Using a sigmoidal resistive transition. Results are compared to the $I(V)$ of a small (1x0.15 μm) device measured at 1.6 THz, with $T_b = 4.2K$; pumping power is determined using isothermal technique. At lower bias, near the optimal operating point a structural difference is apparent. The calculated curve with $P_{LO} = 80$ nW is closest to an optimally pumped one. The inset shows the resistivity profiles for this pumping level.

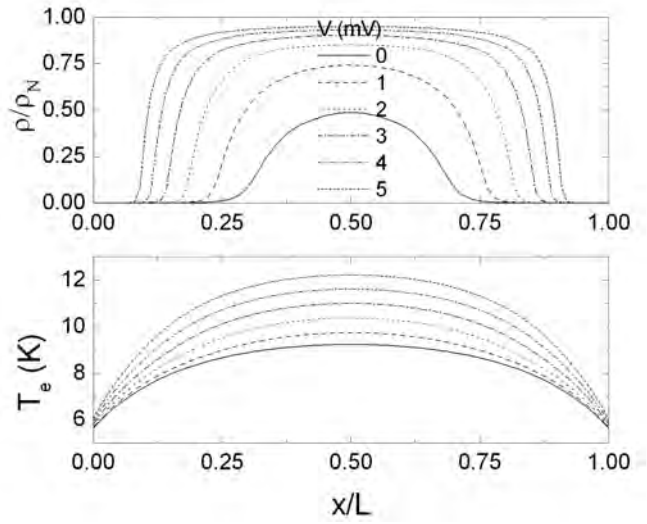

Fig. 2. Electron temperature and local resistivity profiles using the intrinsic resistive transition.

Recently, optimising the contacts between the antenna and the NbN film, by cleaning and inserting a NbTiN interlayer, has virtually doubled sensitivity [3]. This clearly shows the importance of contacts and argues for their involvement in modelling efforts. The phonon temperature at the boundaries equals the bath temperature, following previous modelling [5]. For the electron temperature however, an exponential decay under the contacts is assumed. This conserves the heat flow of the electrons diffusing into the NbTiN and Au, yet involves the contact transparency qualitatively. The boundary condition reads $\frac{d}{dx}T_e(x=0) = \frac{T_e(x=0)-T_b}{l}$. We approximate the decay length with $l = \sqrt{\frac{R_c}{R_\square}} \propto \frac{1}{\sqrt{Tr}}$. For a transparency previously found to be $Tr \approx 0.05$ [4], the thermal decay length is in the order of 5 nm.

Due to the mixed nature of the HEB, with spatial dependent superconductivity, the electronic heat capacity is highly position dependent. Since our interest primarily goes to the role of the resistive transition we take out this complicating factor by assuming a normal state heat capacity and thermal conductance [11]. The phonon heat capacity is assumed close to the Debye model. Experimentally obtained parameters for the NbN film are used for numerical evaluation [6], [7].

III. Resistive Transition

The last step in characterising the HEB's response is translating the knowledge of temperature profiles into the resistance and subsequent $I(V)$ curves. This last step is perhaps the most delicate, and yet essential for validating assumptions used, analysing the response and understanding the physical mechanisms. Therefore, in analysing the HEB, we choose this resistive transition to be a starting point.

From a microscopic view, the resistive transition is a result of many processes, such as flux flow, vortex-antivortex unbinding and material inhomogeneities. Introducing these various processes in a macroscopic heat balance equation is impractical.

In recent modelling a sigmoidal transition has been used, which was fitted to approximate the device transition [2],

$$\frac{\rho(T)}{\rho_N} = \frac{1}{1 + e^{-(T-T_c)/\Delta T_c}} \tag{3}$$

and hence these dynamic microscopics and material properties have been reduced to a T_c, ΔT_c set. This simplification proved to be valuable and gave insight in the formation of resistance, and the subsequent characterisation of $I(V)$ curves and the mixing mechanism [1], [5].

Qualitatively the picture is of a LO power induced bell-shaped resistivity profile, rising fastest in the middle of the bridge, see inset of Fig. 1. Subsequently mixing was found to be most effective in the middle of the bridge.

The downside of models using a sigmoidal transition is that they structurally underestimate the current, thus failing to predict pumped $I(V)$ at low bias, near the optimal operating point, see Fig. 1. The first step in tackling these problems and gain a deeper understanding of the device physics is to choose a better resistive transition. Secondly the LO power needed to pump the device differs significantly between model prediction and experiment, which is partly attributed to simplifications and input parameter accuracy.

Recently, we have learned that the resistive transition of a NbN film without contacts, i.e. the intrinsic film transition, is not sigmoidal, and shows a much sharper onset, see the inset in Fig. 3. The device transition is dominated by contact effects, which do not play a role under operation, since the contacts remain superconducting. The intrinsic transition seems to be a proper choice for describing the local $\rho(T(x))$.

The results of using the intrinsic transition are shown in Fig. 2 and Fig. 3. First of all the electron temperature profiles do not deviate largely from the results previously found, as expected [2]. Note that the electron temperature being higher than the bath temperature at the edges is the result of our choice of the boundary conditions.

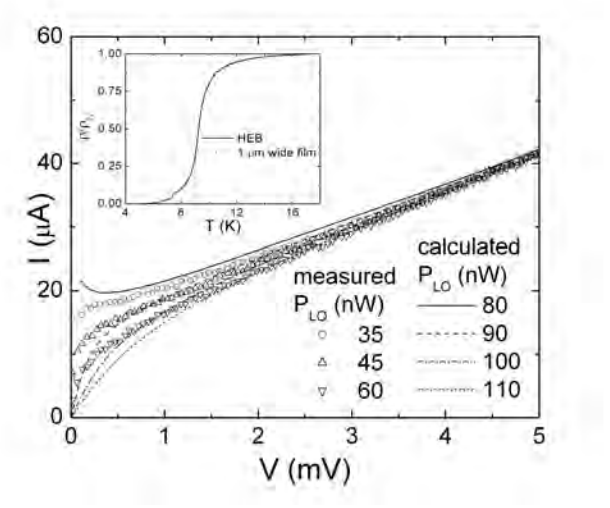

Fig. 3. Modelled and experimental pumped $I(V)$ using the intrinsic resistive transition. The inset shows the difference between the device and film transition.

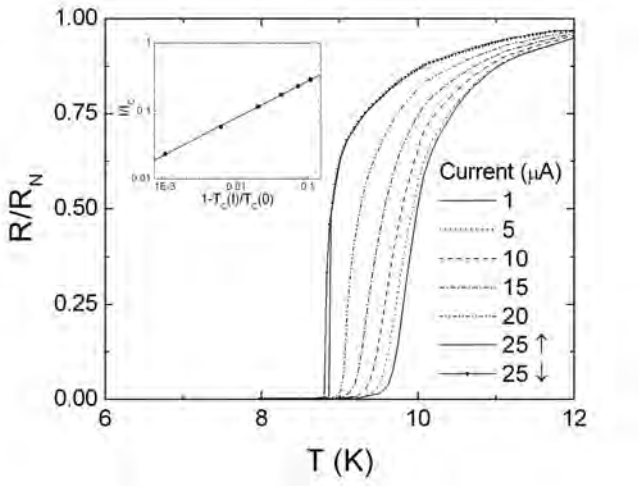

Fig. 4. The intrinsic resistive transition as a function of applied DC bias current of a 1 μm wide processed NbN film. Effectively the critical temperature shifts with increasing bias, and the steepness changes little. The influence of the current on the resistive transition is indicated in the inset, giving $\gamma = 0.54$.

The sharper onset of the intrinsic transition affects the resistivity profiles in the sense that local resistivity is more pronounced at comparable pumping power. Qualitatively the view put forward previously [1], [2] remains valid.

The intrinsic transition shows only marginal improvement for the current-voltage characteristic, and does not capture the device behaviour qualitatively at low bias, where the response is known to be optimal.

IV. Current Dependence

Resistance at the onset of the $\rho(T)$ curve is largely dominated by vortex related behaviour. With increasing electron temperature resistance appears due to vortex-antivortex pair creation, flux flow and phase slip events. These processes depend on the current density [10], hence the local resistivity is an intrinsic current-dependent quantity. Since these processes also depend on material properties, including pinning sites and inhomogeneities, an empirical determination of the resistive transition in the presence of a current is needed.

The intrinsic transition is measured for different DC current bias and shown in Fig. 4. Firstly, the $R(T, I)$ curve shifts, and the apparent downshift of T_c follows the empirical relation

$$\frac{I}{I_c} = (1 - \frac{T_c(I)}{T_c(0)})^{\gamma} \tag{4}$$

for $\gamma = 0.54$, see the inset in Fig. 4. We ignore the small change in the steepness of the resistive transition for different current bias. The shift due to current was first put forward in modelling [9]. Later on the sigmoidal transition, based on the device transition, was extended using a current-dependent critical temperature [5]. Yet the role of current in the intrinsic transition remained underexposed.

The local resistivity profile, calculated using the intrinsic, current dependent resistive transition, is shown in Fig. 5. Again bell-shaped resistivity profiles arise, and the previous conclusions concerning the mixing mechanism remain valid. Yet the resistivity profile is now not only primarily LO-power (and secondarily DC power) induced but also strongly affected by current.

In Fig. 6, we see that the predicted $I(V)$ curves almost fully correspond to the measured curves. For high bias as well as for low bias the model closely follows the measured curves. We achieve a similar result for larger devices.

This unequivocally illustrates that a proper choice of $\rho(T, I)$ is the most pivotal decision in modelling the HEB. We have seen the choice of resistive transition evolve from a sigmoidal transition, approximating the device transition, to the usage of the intrinsic film transition. Yet this change did not have strong effect on the current-voltage characteristics. Only when properly using the current dependence a good agreement is found. This shows that the $I(V)$ is dominated by a good choice of $\rho(T, I)$, not $\rho(T)$, which is in agreement with recent experimental results [12]. Hence device resistance is the result of the interplay between pumping as well as DC power, current, material parameters and the resistive transition: $R = \frac{1}{A}\int_0^L \rho(x, T_e(P_{LO}, P_{DC}), I)dx$.

The current dependence being identified as the dominant choice in modelling the HEB signals a new framework for analysing the device response. The physical behaviour at and around the optimal operating point is much more current oriented than previously assumed. This sheds a new light at our notion of mixing mechanisms, time-dependent processes, related to the thermal time constants, and noise mechanisms, analogous to the excess noise in transition edge sensors [13].

Practically, we might be using the current-dependence twice. In Eq. 1, we use p_{DC}, the local heating due to the transport current, while in $\rho(T, I)$ the current leads to a shift and change of $R(T)$, which may partially be due to heating. We find strong disagreement between measured curves and model calculations for $p_{DC} = 0$. Hence, we believe that the physics contained in Fig. 4 is much more subtle. The thin

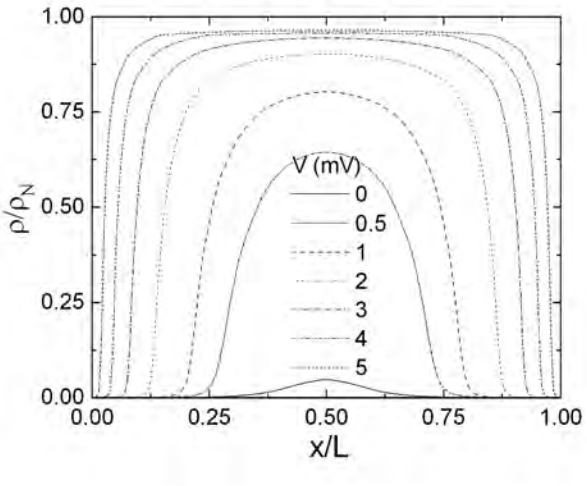

Fig. 5. Local resistivity profiles using the current dependent intrinsic resistive transition. Mixing occurs predominantly in the middle.

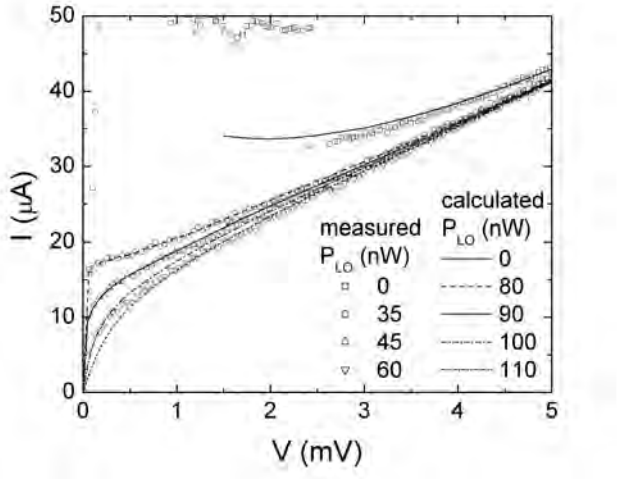

Fig. 6. Using the current dependent intrinsic resistive transition, the model correctly predicts $I(V)$, for high as well as low bias.

NbN films are at the borderline of a superconductor-insulator transition [14], which is known to involve both quasiparticles as well as vortices, topological excitations [15]. Such a two-fluid description will also influence the noise properties [16].

V. Conclusion

Motivated by the inability of present-day HEB models to adequately predict behaviour at low bias, near the optimal operating point, we have analysed different choices for the resistive transition, extending on previous modelling efforts. Using measurements on NbN films, we have replaced sigmoidal transitions, approximating the device transition, with the measured intrinsic film transition. Although this last transition has a significantly different shape, only a marginal improvement was found in predicting current-voltage characteristics. Therefore we have identified the role of current in the intrinsic transition, and, using a $\rho(T, I)$ criterion, our model now correctly predicts the complete $I(V)$ behaviour. Current being identified as a dominant factor in the resistive transition leads to a new view on device response.

Acknowledgements

We thank J. Baselmans for providing the measured $I(V)$ data and A. Baryshev for stimulating discussions. The work is supported partly by RadioNet and partly by INTAS.

References

[1] T.M. Klapwijk, R. Barends, J.R. Gao, M. Hajenius and J.J.A. Baselmans, *Improved superconducting hot electron bolometer devices for the THz range*, Proc. SPIE Vol. 5498, p. 129 (2004).

[2] M. Hajenius, R. Barends, J.R. Gao, T.M. Klapwijk, J.J.A. Baselmans, A. Baryshev, B. Voronov and G. Gol'tsman, *Local resistivity and the current-voltage characteristics of hot electron bolometer mixers*, IEEE Trans. Appl. Sup., in press.

[3] J.J.A. Baselmans, M. Hajenius, J.R. Gao, T.M. Klapwijk, P.A.J. de Korte, B. Voronov and G. Gol'tsman, *Doubling of sensitivity and bandwidth in phonon cooled hot electron bolometer mixers*, Applied. Phys. Letters, **84**, 1958 (2004).

[4] M. Hajenius, J. J. A. Baselmans, J. R. Gao, T. M. Klapwijk, P. A. J. de Korte, B. Voronov and G. Gol'tsman, *Low Noise NbN superconducting Hot Electron Bolometer mixers at 1.9 and 2.5 THz*, Supercond. Sci. Technol. **17**, S224 (2004).

[5] P. Khosropanah, H. Merkel, S. Yngvesson, A. Adam, S. Cherednichenko and E. Kollberg, *A distributed device model for phonon-cooled HEB mixers predicting IV characteristics, gain, noise and IF bandwidth*, Proc. 11^{th} Int. Symp. Space Thz Technology, p 474 (2000); P. Khosropanah, *NbN and NbTiN Hot Electron Bolometer THz Mixers*, Ph. D. Thesis, Chalmers University of Technology (2003).

[6] A.D. Semenov, R.S. Nebosis, Yu.P. Gousev, M.A. Heusinger and K.F. Renk, *Analysis of the nonequilibrium photoresponse of superconducting films to pulsed radiation by use of a two-temperature model*, Phys. Rev. B **52**, 581 (1995).

[7] A.D. Semenov, G.N. Gol'tsman, A. A. Korneev, *Quantum detection by current carrying superconducting film*, Physica C **351**, 349 (2001).

[8] Y. Pellan, G. Dousselin and J. Pinel, *Temperature and Magnetic Field Dependence of NbN Film Resistivity: 3D Weak Localization Effects*, J. Low Temp. Phys. **78**, 63 (1990).

[9] R.S. Nebosis, A.D. Semenov, Yu.P. Gousev and K.F. Renk, *Rigorous Analysis of Superconducting Hot-Electron Bolometer Mixer: Theory and Comparison with Experiment*, Proc. 7^{th} Int. Symp. Space THz Technology, p. 601 (1996).

[10] A.M. Kadin, K. Epstein and A.M. Goldman, *Renormalization and the Kosterlitz-Thouless transition in a two-dimensional superconductor*, Phys. Rev. B **27**, 6691 (1983).

[11] D. Wilms Floet *Hotspot Mixing in THz Niobium Superconducting Hot Electron Bolometer Mixers*, Ph. D. Thesis, Delft University of Technology (2001). Calculations using a powerlaw approximating the superconducting thermal conductance indicate qualitatively equal outcome for a somewhat smaller pumping power.

[12] Z.Q. Yang, M. Hajenius, J.J.A. Baselmans, J.R. Gao , T.M. Klapwijk, B. Voronov, G. Gol'tsman, *Improved sensitivity of NbN hot electron bolometer mixers by vacuum baking*, this conference proceedings.

[13] G.W. Fraser, *On the nature of the superconducting-to-normal transition in transition edge sensors*, Nuclear Inst. and Methods in Physics Research A, **523**, 234 (2004).

[14] H. Su, N. Yoshikawa and M. Sugahara, *Study of electrical conduction properties of NbN thin films using NbN/MgO/NbN double-tunnel junctions*, Supercond. Sci. Technol. **9**, A152 (1996).

[15] V.M. Galitski, G. Refael, M.P.A. Fisher and T. Senthil, *Vortices and quasiparticles near the superconductor-insulator transition in thin films*, cond-mat/0504745.

[16] R.F. Voss, C.M. Knoedler and P.M. Horn, *Phase-slip shot noise at the two-dimensional superconducting transition: evidence for vortices?*, Phys. Rev. B **45**, 1523 (1980).